Society of Production Engineering

ICPES 2025

40th INTERNATIONAL CONFERENCE ON PRODUCTION ENGINEERING - SERBIA 2025

DOI: 10.46793/ICPES25.431V

University of Nis Faculty of Mechanical Engineering

Nis, Serbia, 18 - 19th September 2025

INFLUENCE OF STRUT CROSS-SECTION GEOMETRY ON THE MECHANICAL PROPERTIES OF MSLA-FABRICATED BONE SCAFFOLDS

Aleksandra VELIČKOVIĆ[1], Rajko TURUDIJA[2] *, Jovan ARANĐELOVIĆ[1], Jelena STOJKOVIĆ[1]*

Orcid: 0009-0006-8017-6787; **Orcid:** 0000-0002-6324-5967; **Orcid:** 0000-0001-9653-4119;

Orcid: 0000-0002-8249-2816;

[1] Faculty of Mechanical Engineering, Niš, Serbia, andra0174@gmail.com

*Corresponding author: rajko.turudija@masfak.ni.ac.rs

Abstract: *Severe bone injuries often result in critical-sized defects that exceed the body's natural healing capacity, requiring engineered scaffolds to restore mechanical stability and promote bone regeneration. This study investigates how different strut cross-sectional geometries affect the mechanical properties of 3D-printed bone scaffolds. Six geometries (including square, rhomboid, circular, and three others) were designed and fabricated using Masked Stereolithography (MSLA) technology. Multiple samples of each geometry were produced and tested under uniaxial compression using a universal testing machine. Key parameters analyzed included engineering stress and elastic modulus. Results showed significant variation in mechanical properties depending on the cross-sectional shape. Scaffolds with rectangular strut cross-section exhibited the highest compressive strength of 33.39 MPa, while those with circular strut cross-section recorded the lowest value of 27.38 MPa. Additionally, scaffolds with a circular strut cross-section exhibited the highest elastic modulus of 1774.3 N/mm², while scaffolds with a cross-shaped strut cross-section exhibited the lowest elastic modulus of 1153.7 N/mm². These findings highlight the importance of geometric optimization in scaffold design for improved mechanical stability.*

Keywords: *lattice-like scaffolds, strut cross-section, mechanical properties, MSLA*

1. INTRODUCTION

At the global level, the incidence of bone fractures, defects, and tumors is steadily increasing [1]. Each year, approximately four million surgical procedures are performed to address bone loss using grafts and/or bone tissue replacements [2]. Although bone tissue has the capacity to regenerate, defects exceeding a critical size (approximately >2 cm) often exhibit significantly impaired healing and fail to repair spontaneously [3]. Tissue engineering employs integrated, multidisciplinary strategies to enhance or replace damaged biological tissues [4]. Within this field, scaffolds play a central role: they not only provide a temporary structure to support cell adhesion, proliferation, and differentiation, but also facilitate the formation of new tissue. Furthermore, scaffolds interact with cells and bioactive molecules that regulate tissue remodeling. As a result, scaffolds are commonly designed to mimic the structure and composition of the extracellular matrix (ECM), thereby reestablishing communication between cells and the ECM, and ultimately promoting effective tissue regeneration [3]. The present study aims to evaluate the mechanical properties of such scaffolds.

The properties of bone scaffolds largely depend on their microstructure. Scaffold microstructures can be classified into three groups. First, scaffolds formed from periodic, regular lattice structures (Figure 1a), which are constructed from repeating units (cells) and are primarily used in the early stages of bone scaffold development. Second, scaffolds formed from irregular and non-periodic structures (Figure 1b), which closely resemble natural bone and may represent an ideal replacement for damaged bone tissue. Finally, scaffolds formed from bioinspired (bionic) microstructures (Figure 1c), such as Triply Periodic Minimal Surfaces (TPMS), which are widely employed in bone scaffold design [5].

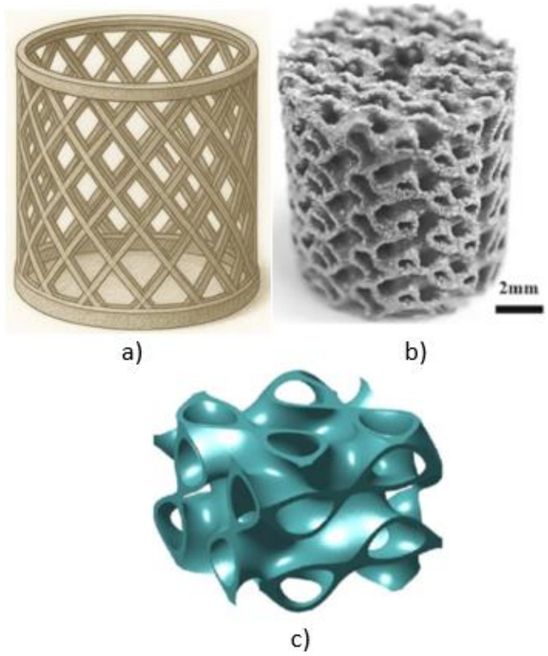

Figure 1. a) Lattice-like, b) Irregular and non-periodic, c) TPMS bone scaffold structures [5]

An ideal scaffold should be biodegradable, biocompatible, bioactive, osteoconductive, osteoinductive, and non-toxic, while also possessing optimal mechanical properties—such as stiffness, pore size, surface topology, and load-bearing capacity—to promote successful cell proliferation and osteogenic differentiation [1]. The main limitations in scaffold application include insufficient vascularization, inadequate mechanical strength, and difficulties in managing bone infections [6]. Biomaterials, which form the fundamental components of scaffolds, play a crucial role in bone tissue engineering. Materials such as metals, natural and synthetic polymers, ceramics, and their composites have been widely used for decades as scaffold materials in biomedical fields [4].

To be suitable for clinical use, scaffolds must comply with established mechanical performance standards. Numerous experimental studies have investigated the mechanical response of porous scaffolds through uniaxial compression testing [9], [10], [12] – [17], while other research has employed computational structural analyses to predict their behaviour under various loading conditions [7], [8], [10], [12] – [15], [17] – [19]. Taken together, these studies highlight consistent trends, showing that both scaffold geometry [10], [12], [15] – [17] and manufacturing parameters [8], [12] – [14] play a crucial role in determining overall mechanical behaviour.

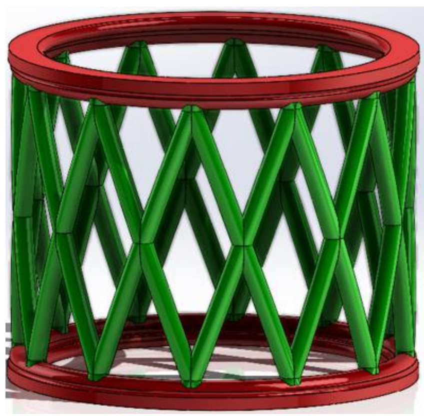

Figure 2. Lattice like scaffold

A review of the literature clearly highlights the need for further research into the structure and geometry of scaffolds, particularly lattice-like scaffolds composed of periodic, regular structures. One such scaffold design, developed and presented by the authors in a previous study [20], was specifically intended for the treatment of small segmental bone defects (Figure 2). The scaffold was fabricated using Masked Stereolithography (MSLA) 3D printing technology. This type of scaffold remains insufficiently investigated in terms of its mechanical behavior, the optimization of various strut shapes, and the influence of strut cross-sectional geometry on its overall mechanical performance. The aim of this study is to advance knowledge regarding the mechanical characteristics of this type of scaffold by examining how strut cross-sectional geometry affects its mechanical behavior.

This paper includes an introduction and literature review, a description of the methodology, a presentation and discussion of the results, and a summary of the main conclusions.

2. METHODOLOGY

The aim of this research is to expand the understanding of the mechanical characteristics of lattice-structured scaffolds by analyzing the influence of strut cross-section on their mechanical performance.

The lattice scaffold models described in the previous section were designed for small bone defect segments and subjected to uniaxial compression testing to evaluate their mechanical performance. Twelve lattice scaffold models representing six different strut geometries (square, rhomboid, circular, two rectangular, and cross-shaped) were fabricated – two models for each geometry. These models were designed in SolidWorks CAD software (SolidWorks 2023) using fully parametric modeling. The scaffolds were constructed from beams at the top and bottom of the outer frame, connected by vertical struts. The outer frame beams have a diameter of 36 mm. The 12 vertical struts, evenly spaced around the frame, were cut at an angle of 35°. According to these dimensions, the scaffold is small, with a height of 30 mm and width of 40 mm. The scaffold models were made with six different cross-sectional shapes of the struts, oriented perpendicular to the strut direction (Figure 3). The cross-sectional areas were kept identical at 2.5 mm^2 to isolate the effect of shape on mechanical performance.

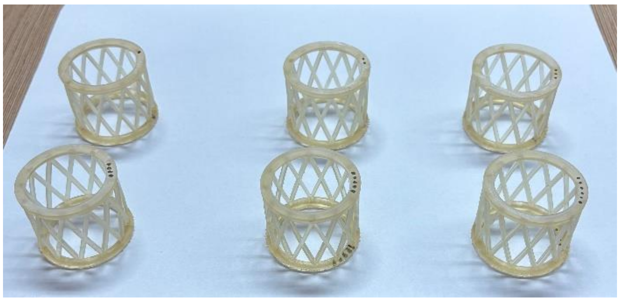

Figure 3. Lattice like scaffold used for the experiments

The previously mentioned scaffold models were fabricated using MSLA (Masked Stereolithography) 3D printing technology, which enables high precision and fine detail in complex microstructures. MSLA technology utilizes a UV LCD screen to mask individual layers of photopolymer resin, allowing selective curing of the material and achieving high printing resolution.

Figure 4. Anycubic Photom M3 Plus 3D printer

The scaffold models were prepared for printing using Anycubic Photon Workshop software (v.3.1.4), which facilitates optimization of printing parameters and precise control over the CAD model geometry. The scaffolds were printed on an Anycubic Photon M3 Plus 3D printer (Figure 4), which enables the production of scaffolds with high dimensional accuracy and microstructure control. This 3D printer features a build volume of 245 × 197 × 122 mm, an LCD screen resolution of 5760 × 3600 pixels, and a layer resolution of 34 microns. Additional technical specifications of the printer are provided in the Table 1. The material used for model fabrication is ECO UV RESIN Black — a resin whose properties, detailed in the Table 2, contribute to the stability and mechanical resistance of the scaffold.

Table 1. Mechanical properties of Anycubic Photom M3 Plus 3D printer [21]

Mechanical Properties	Value
Exposure screen	9.25 inch monochrome screen
Printing volume	5.9 liters
Printing platform	Laser engraved aluminum alloy platform
Printing speed	≤100 mm/hour
Rated power	144W
Mechanical Properties	**Value**
Machine weight	~12kg
Machine dimensions	475 x 360 x 290 mm
Machine leveling	4-point manual leveling

Table 2. Material properties of ECO UV RESIN [22]

Property	Value
Material type	ECO UV RESIN
Manufacturing process	Masked Stereolithography (MSLA)
Color	Black
Tensile strength	59 – 70 Mpa
Elongation at break	11-20%
Density	1.05-1.25 g/cm3
Viscosity (25°C)	300 mPas
Print Layer Thickness	from 35 microns
Volume	1l
Recommended baking time for layers	6-10 seconds

Since the aim of this research is to analyze the influence of scaffold cross-section on their mechanical performance, quasi-static uniaxial compression tests were performed. These tests evaluate the behavior and mechanical properties of scaffold materials or structures under compressive force applied in a single direction. Additionally, the tests enable precise analysis of the scaffold's mechanical properties under compression, which is essential for optimizing its design and material selection. The quasi-static uniaxial compression tests were conducted on a Shimadzu Table-top AGS-X universal testing machine (Shimadzu, Kyoto, Japan) equipped with a 10 kN load cell. Testing was carried out at a crosshead speed of 0.5 mm/min with a speed accuracy of 0.1%. The universal testing machine and the test setup are shown in the Figure 5, while the technical specifications of the machine are presented in the Table 3. During the tests, data on force as a function of crosshead displacement (useful for generating force-displacement diagrams) were recorded at specific intervals and collected using Shimadzu TrapeziumX software at a sampling frequency of 100 Hz.

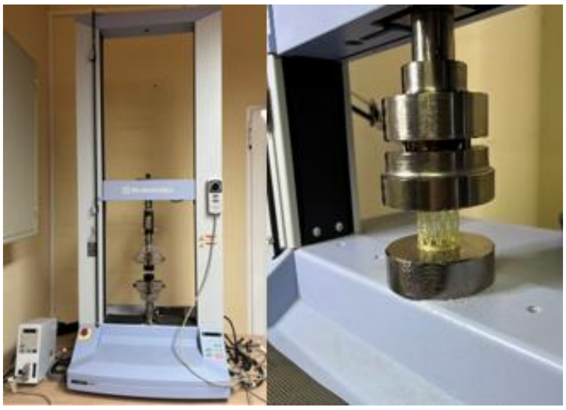

Figure 5. Shimadzu Table-top AGS-X 10 kN universal testing machine (left), experiment setup (right)

Table 3. Shimadzu Table-top AGS-X 10 kN universal testing machine characteristics [23]

Mechanical Properties	Value
Brand	Shimadzu
Model	Table-top AGS-X 10 kN
Weight	85 kg
Power	1.2 kW
Max load/capacity	10 kN
Dimensions	W653 × D520 × H1603 mm
Crosshead speed range	0.001 to 1000 mm/min
Crosshead speed accuracy	0.1%
Crosshead—table distance (tensile stroke)	1200 mm (760 mm, MWG)
Data capture rate	1000 Hz max

After the quasi-static uniaxial compression tests, experimental results consisting of stress-strain curves were obtained. Six scaffold models, differing in strut cross-section (square, rhomboid, circular, two rectangular, and cross-shaped), were subjected to these tests. Two independent tests were performed for each scaffold model to ensure the reliability and repeatability of the results. Based on this, the total number of quasi-static uniaxial compression tests conducted was 12.

3. RESULTS AND DISCUSSION

In the previous section, all six scaffold models, each characterized by a distinct strut cross-section, were described in detail. These models were subjected to quasi-static uniaxial compression tests (performed twice for each scaffold model) to evaluate the influence of strut cross-section on their mechanical properties. The tests yielded specific experimental results that served as the basis for generating the corresponding stress-strain curves. Figure 6 presents these curves (i.e., the relationship between stress and strain) obtained after performing all quasi-static uniaxial compression tests on the twelve tested scaffold specimens. Table 4 summarizes selected numerical data from the testing of all six scaffold models in two repeated trials. The table includes the maximum force recorded, the maximum stress, Young's modulus, and the coefficient of determination (R^2) for each scaffold model.

The stress–strain curves presented in Figure 6 clearly illustrate the differences in maximum stress values, the post-peak behavior (fracture of the scaffold models), and the variations in the deformation zone observed during the quasi-static uniaxial compression tests conducted on the twelve tested scaffold specimens. All these differences are directly related to the cross-sectional shape of the struts (circular, square, rhomboid, two rectangular, and cross-shaped). Scaffold models with rectangular strut cross-sections (4-1, 4-2, 5-1, and 5-2) reach the highest stress values and exhibit a steeper initial slope of the curve, which directly indicates greater stiffness of these models. Scaffolds with rhomboid and cross-shaped strut cross-sections (3-1, 3-2, 6-1, and 6-2) exhibit relatively high stress values and are characterized by an extended deformation zone prior to fracture, which makes them more resistant to sudden failure.

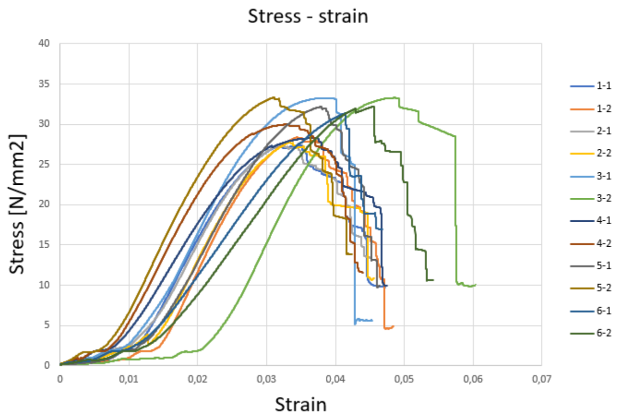

Figure 6. Stress–strain curves obtained after quasi-static uniaxial compression tests

Table 4. Numerical data obtained from testing all six scaffold models in two repeated trials

Scaffold models	F_{max} [N]	σ_{max} [N/mm^2]	E [N/mm^2]	R^2
1-1	821.54	27.38	1583.2	0.9993
1-2	852.26	28.41	1774.3	0.9992
2-1	830.38	27.68	1543.7	0.9984
2-2	834.84	27.83	1666.1	0.9993
3-1	997.82	33.26	1645.3	0.9993
3-2	998.72	33.29	1688.5	0.999
4-1	848.21	28.27	1368.6	0.9996
4-2	900.14	30.01	1638.1	0.9997
5-1	966.00	32.20	1523.8	0.9993
5-2	1001.6	33.39	1710.7	0.999
6-1	941.24	31.38	1180	0.9998
6-2	965.96	32.199	1153.7	0.9994

After reaching maximum stress, they gradually lose load-bearing capacity and are able to withstand loading for a longer period. In contrast, scaffolds with circular and square strut cross-sections (1-1, 1-2, 2-1, and 2-2) show the lowest stress values and have a more moderate initial slope on the curve, clearly indicating lower stiffness.

After reaching their peak stress, scaffolds with circular and square strut cross-sections (1-1, 1-2, 2-1, and 2-2) exhibit a sharp drop in stress, leading to a brittle fracture mode, whereas scaffolds with rhomboid and cross-shaped strut cross-sections (3-1, 3-2, 6-1, and 6-2) retain a gradual decrease in stress and an extended deformation phase.

Table 4 presents the maximum force and stress values, elastic modulus, and coefficient of determination for all six scaffold models with different strut cross-sectional shapes (circular, square, rhomboid, two rectangular, and cross-shaped) in two repeated tests. The results indicate significant differences in mechanical performance depending on the cross-sectional geometry, despite all specimens being tested under identical conditions.

Scaffolds with rhomboid and rectangular strut geometries–model 3 (998.72 N) and model 5 (1001.6 N) – achieved the highest force values. Both scaffolds also exhibited the highest stress values, 33.29 N/mm² and 33.39 N/mm², indicating exceptional load-bearing capacity. In contrast, the lowest force values were recorded for scaffolds with circular and square strut cross-sections, model 1 (821.54 N) and model 2 (830.38 N), which also displayed the lowest stress values, 27.38 N/mm² and 27.68 N/mm², reflecting lower load capacity and reduced resistance to compression. Based on these results, a positive correlation between maximum force and maximum stress can be established. The elastic modulus values also vary depending on the strut geometry of the scaffolds. The highest elastic modulus values were observed for scaffolds with circular and rectangular strut cross-sections, model 1 (1774.2 N/mm²) and model 5 (1710.7 N/mm²), while the lowest elastic modulus was recorded for the scaffold with a cross-shaped strut cross-section, model 6 (1180 N/mm²). These findings demonstrate that certain strut geometries can simultaneously provide high strength and stiffness, whereas others offer greater elasticity at the expense of load-bearing capacity.

Based on all the presented results, it can be concluded that the geometry of the strut cross-section significantly impacts the mechanical performance of the scaffolds. Scaffolds with rhomboid and rectangular strut cross-sections (model 3 and 5) exhibited the best mechanical performance, showing an optimal balance of maximum force, stress, and elastic modulus, along with exceptional load-bearing capacity and good elasticity. In contrast, scaffolds with circular, square, and cross-shaped strut cross-sections (models 1, 2, and 6) showed the weakest mechanical performance — models 1 and 2 due to their lowest load-bearing capacity, and model 6 due to its lowest elastic modulus, indicating the greatest brittleness.

4. CONCLUSION

In this study, the influence of six different strut cross-sectional geometries (circular, square, rhomboid, two rectangular, and cross-shaped) on the mechanical performance of lattice scaffolds intended for small bone defect segments was thoroughly investigated. Twelve scaffold models (two for each geometry) were fabricated using an Anycubic Photon M3 Plus 3D printer with MSLA technology and tested on a Shimadzu Table-top AGS-X machine under quasi-static uniaxial compression.

The experimental results confirmed that strut cross-sectional geometry significantly affects scaffold performance in terms of load-bearing capacity, stiffness, strength, deformation behaviour, and fracture mode. Scaffolds with rhomboid and rectangular strut cross-sections exhibited the highest maximum force and stress values while simultaneously maintaining optimal elasticity. These scaffolds are characterized by exceptional load-bearing capability, making them particularly suitable for applications requiring high load capacity combined with a certain level of deformability. In contrast, scaffolds with circular and square strut cross-sections recorded the lowest force and stress values, and thus the lowest load-bearing capacity, along with a greater tendency toward brittle fracture. Scaffold models with cross-shaped strut cross-sections had the lowest elastic modulus, indicating increased flexibility but significantly lower resistance to load. Analysis of the stress–strain curves further revealed that the geometry of the strut cross-section influences not only the maximum values of stress, force, and elastic modulus but also the post-fracture behaviour of the scaffolds. This influence is manifested as either a sudden loss of load-bearing capacity, as observed in scaffolds with circular and square strut cross-sections, or a gradual decrease in load, as in scaffolds with rhomboid and cross-shaped strut cross-sections.

The presented test results indicate that the choice of strut cross-sectional geometry can be a critical parameter in designing scaffolds for specific applications. This study forms part of a broader investigation aimed at identifying the mechanical property patterns of this particular lattice-structured scaffold. Future research will focus on incorporating numerical methods, such as finite element analysis (FEA), to more accurately assess stress distribution and optimize the structure for improved scaffold performance.

ACKNOWLEDGEMENT

The research activities are financed by the Ministry of Science, Technological Development and Innovation of the Republic of Serbia (Contract No. 451-03-47/2023-01/200109).

REFERENCES

[1] Seunghun S. Lee, Xiaoyu Du, Inseon Kim, Stephen J. Ferguson, “Scaffolds for bone-tussue engineering, Matter”, Vol. 5, Issue 9, pp. 2722-2759, 2022.

[2] Tongyu Zhu, Hongbo Zhou, Xiaojing Chen, Yuanjing Zhu, “Rcent advances of responsive scaffolds in bone tissue engineering, Frontiers”, Vol. 11, pp. 534–538, 2023.

[3] Chang Xu, Zhize Liu, Xi Chen, Yang Gao, Wenjun Wang, Xijing Zhuang, Hao Zhang, Xufeng Dong, “Bone tissue engineering scaffold materials: Fundamentals, advances, and challenges”, ScienceDirect, Vol. 35, pp. 109-197, 2024.

[4] Huawei Qu, Hongya Fu, Zhenyu Hana, Yang Sun, “Biomaterials for bone tissue engineering scaffolds: a review”, Publishing, Vol. 9, pp. 26252-26262, 2019.

[5] Yi Huo, Yongtao Lu, Lingfei Meng, Jiongyi Wu, Tingxiang Gong, Jia’ao Zou, Sergei Bosiakov, Liangliang Cheng, “A Critical Review on the Design, Manufacturing and Assessment of the Bone Scaffold for Large Bone Defects”, PubMed Central, Vol. 9, pp. 404–411, 2021.

[6] Yuchun Liu, Jing Lim, Swee-Hin Teoh, “Review: development of clinically relevant scaffolds for vascularised bone tissue engineering”, PubMed, Vol. 31, pp. 688-705, 2013.

[7] M. A. Wettergreen, B. S. Bucklen, B. Starly, E. Yuksel, W. Sun, and M. A. K. Liebschner, “Creation of a unit block library of architectures for use in assembled scaffold engineering,” Comput. Des., vol. 37, no. 11, pp. 1141–1149, Sep. 2005.

[8] G. Ryan, P. McGarry, A. Pandit, and D. Apatsidis, “Analysis of the mechanical behavior of a titanium scaffold with a repeating unit-cell substructure,” J. Biomed. Mater. Res. Part B Appl. Biomater., vol. 90B, no. 2, pp. 894–906, Aug. 2009.

[9] G. E. Ryan, A. S. Pandit, and D. P. Apatsidis, “Porous titanium scaffolds fabricated using a rapid prototyping and powder metallurgy technique,” Biomaterials, vol. 29, no. 27, pp. 3625–3635, Sep. 2008

[10] M. Ramu, M. Ananthasubramanian, T. Kumaresan, R. Gandhinathan, and S. Jothi, “Optimization of the configuration of porous bone scaffolds made of Polyamide/Hydroxyapatite composites using Selective Laser Sintering for tissue engineering applications,” Biomed. Mater. Eng., vol. 29, no. 6, pp. 739–755, Jan. 2018.

[11] C. Shi, N. Lu, Y. Qin, M. Liu, H. Li, and H. Li, “Study on mechanical properties and permeability of elliptical porous scaffold based on the SLM manufactured medical Ti6Al4V,” PLoS One, vol. 16, no. 3, p. e0247764, Mar. 2021.

[12] M. Asadi-Eydivand, M. Solati-Hashjin, and N. A. Abu Osman, “Mechanical behavior of calcium sulfate scaffold prototypes built by solid free-form fabrication,” Rapid Prototyp. J., vol. 24, no. 8, pp. 1392–1400, Nov. 2018.

[13] S. Eshraghi and S. Das, “Micromechanical finite-element modeling and experimental characterization of the compressive mechanical properties of polycaprolactone–hydroxyapatite composite scaffolds prepared by selective laser sintering for bone tissue engineering,” Acta Biomater., vol. 8, no. 8, pp. 3138–3143, Aug. 2012.

[14] S. Cahill, S. Lohfeld, and P. E. McHugh, “Finite element predictions compared to experimental results for the effective modulus of bone tissue engineering scaffolds fabricated by selective laser sintering,” J. Mater. Sci. Mater. Med. 2009 206, vol. 20, no. 6, pp. 1255–1262, Feb. 2009.

[15] J. Wieding, R. Souffrant, W. Mittelmeier, and R. Bader, “Finite element analysis on the biomechanical stability of open porous titanium scaffolds for large segmental bone defects under physiological load conditions,” Med. Eng. Phys., vol. 35, no. 4, pp. 422–432, Apr. 2013.

[16] Z. Xu, A. M. Omar, and P. Bartolo, “Experimental and Numerical Simulations of 3D-Printed Polycaprolactone Scaffolds for Bone Tissue Engineering Applications,” Mater. 2021, Vol. 14, Page 3546, vol. 14, no. 13, p. 3546, Jun. 2021.

[17] S. Naghieh, M. R. Karamooz Ravari, M. Badrossamay, E. Foroozmehr, and M. Kadkhodaei, “Numerical investigation of the mechanical properties of the additive manufactured bone scaffolds fabricated by FDM: The effect of layer penetration and post-heating,” J. Mech. Behav. Biomed. Mater., vol. 59, pp. 241–250, Jun. 2016.

[18] C. Shi, N. Lu, Y. Qin, M. Liu, H. Li, and H. Li, “Study on mechanical properties and permeability of elliptical porous scaffold based on the SLM manufactured medical Ti6Al4V,” PLoS One, vol. 16, no. 3, pp. 1–17, 2021.

[19] Z. Xu, A. M. Omar, and P. Bartolo, “Experimental and Numerical Simulations of 3D-Printed Polycaprolactone Scaffolds for Bone Tissue Engineering Applications,” Materials (Basel)., vol. 14, no. 13, 2021.

[20] J. R. Milovanovic, M. S. Stojkovic, K. N. Husain, N. D. Korunovic, and J. Arandjelovic, “Holistic approach in designing the personalized bone scaffold: The case of reconstruction of large missing piece of mandible caused by congenital anatomic anomaly,” J. Healthc. Eng., vol. 2020, 2020.

[21] Anycubic photon M3 Plus, available at: https://store.anycubic.com/products/photon-m3-plus, accessed: 10.08.2025.

[22] Anycubic-Grey/Gray Eco Plant-Based UV Resin 0.5kg, available at: https://anycubic.biz/grey-gray-eco-plant-based-uv-resin-anycubic-05kg, accessed: 10.08.2025.

[23] Rajko Turudija, Miloš Stojkovic, Jelena R. Stojkovic, Jovan Arandelovic and Dragan Marinkovic, “Stiffness of Anatomically Shaped Lattice Scaffolds Made by Direct Metal Laser Sintering of Ti-6Al-4V Powder: A Comparison of Two Different Design Variants”, Metals. Eng., vol. 2024, 2024.